Review

Biomechanical and Aerodynamic Modulation for Sinonasal Homeostasis in Craniofacial Orthopedics: A Comprehensive Review of RAMPA Therapy

Yasushi Mitani , Yuko Okai-Kojima , Mohammad Moshfeghi , Bumkyoo Choi * , Yoshiya Hashimoto

Posted Date: 20 May 2026

doi: 10.20944/preprints202605.1331.v1

Keywords: RAMPA therapy; mechanotransduction; Bone Morphogenetic Protein-2 (BMP-2); computational fluid dynamics (CFD); shear-thinning mucus rheology; sinonasal homeostasis; craniofacial remodeling

 doi:10.20944/preprints202605.1331.v1

Review

Biomechanical and Aerodynamic Modulation for Sinonasal Homeostasis in Craniofacial Orthopedics: A Comprehensive Review of RAMPA Therapy

Yasushi Mitani [1], Yuko Okai-Kojima [2], Mohammad Moshfeghi [3], Bumkyoo Choi [3,*] and Yoshiya Hashimoto [4]

[1] Private Practice, Codomo Clinic, Tokyo 180-0004, Japan
[2] Private Practice, Children and Women Dental Clinic, Tokyo 106-0046, Japan
[3] Department of Mechanical Engineering, Sogang University, 35 Baekbeom ro, Mapogu, Seoul 04107, Republic of Korea
[4] Department of Biomaterial, Osaka Dental University, Hirakata 573-1121, Japan
* Correspondence: bkchoi@sogang.ac.kr; Tel.: +82-10-2717-8639

Abstract

Background: Maxillary hypoplasia and skeletal Class III malocclusion are deeply intertwined with upper airway constriction and paranasal sinus dysfunction. Conventional orthopedic interventions often struggle to achieve true 3D skeletal translation without inducing undesirable rotational side effects. The Right Angle Maxillary Protraction Appliance (RAMPA) therapy offers a biomimetic and mechanotherapeutic approach, focusing on anterosuperior protraction to restore both structural harmony and respiratory function. Methods: This feature paper systematically reviews the multi-disciplinary evidence supporting RAMPA therapy, synthesizing findings from recent computational and clinical studies. We examine Finite Element Method (FEM) simulations detailing sutural mechanotransduction and osteogenic "BMP-2 Trigger Zones", Computational Fluid Dynamics (CFD) utilizing shear-thinning rheological models for two-phase air-mucus interactions, and large-cohort CBCT and Coben analyses quantifying longitudinal growth. Results: FEM studies confirm that RAMPA, especially when combined with intraoral devices (e.g., gHu-1, VomPress, Hybrid), achieves predictable anterosuperior displacement and concentrates tensile stress to trigger molecular bone remodeling. CFD simulations reveal that this precise skeletal remodeling optimizes wall shear stress (WSS) and actively facilitates paranasal mucus clearance via enhanced suction and shear-thinning effects. Clinically, RAMPA induces a 1.2-fold acceleration in natural sinonasal growth velocity. Furthermore, volumetric gains are distinctively pronounced in patients with pre-existing empyema (61.2% increase) compared to those with clear sinuses (18% increase), indicating rapid pathophysiological obstruction relief. Conclusions: By integrating controlled biomechanical forces with fluid-dynamic airway optimization, RAMPA therapy acts as a mechanotherapeutic modulator. It bridges the gap between mechanical intervention, molecular signaling, and physiological homeostasis, offering a comprehensive paradigm for pediatric craniofacial and respiratory restoration.

Keywords: RAMPA therapy; mechanotransduction; Bone Morphogenetic Protein-2 (BMP-2); computational fluid dynamics (CFD); shear-thinning mucus rheology; sinonasal homeostasis; craniofacial remodeling

1. Introduction

1.1. Craniofacial and Sinonasal Growth as Determinants of Pediatric Airway Function

As early as 1969, Moss and Salentijn [1] highlighted that craniofacial growth is governed by two functional matrices—periosteal (muscles, teeth) and capsular (neural and oronasopharyngeal

 doi:10.20944/preprints202605.1331.v1

spaces)—each exerting distinct influences on skeletal units. They proposed that periosteal matrices directly modify bone form, whereas capsular matrices alter cranial component position through volumetric expansion, making facial growth a combined process of spatial translation and morphological change. Building on this functional paradigm, McNamara [2] further illustrated that upper airway obstruction is associated with characteristic skeletal and dental configurations—most notably a steep mandibular plane—and that removal of the obstruction can modify subsequent facial growth patterns, reinforcing the functional relationship between respiratory mode and craniofacial development. Later, Solow et al. [3] reported that in 24 children aged 7–9, larger craniocervical angles were consistently associated with smaller mandibular dimensions, mandibular retrognathism, and increased mandibular inclination. They found that obstructed nasopharyngeal airways—defined by reduced pm-ad_2 distance and elevated nasal respiratory resistance—were linked to the same craniofacial pattern, concluding that craniofacial morphology, head posture, and airway resistance show predictable associations even in children without overt airway obstruction.

Subsequent clinical evidence reinforced the influence of airway function on craniofacial development. Rosetti Lessa et al. [4] found that mouth-breathing children (ages 6–10) exhibited greater mandibular plane inclination (SN.GoGn) and reduced posterior-to-anterior facial height ratios, indicating a more vertical growth pattern. Kim et al. [5] added further evidence by demonstrating that preadolescent children with retrognathic mandibles exhibit significantly smaller total pharyngeal airway volumes than those with normal anteroposterior skeletal relationships, reinforcing the link between mandibular position and airway morphology. Indriksone and Jakobsone [6] further showed that in 276 healthy adults aged 17–27 years, craniofacial factors such as SNA angle, gender, and adenoid presence explained only 23% of the variability in nasopharyngeal airway volume, with weak but significant correlations between SNB angle and both oropharyngeal volume ($r = 0.144$) and minimal cross-sectional area ($r = 0.182$). These findings suggest that craniofacial morphology alone does not fully determine airway dimensions. Complementing this, Chuang and colleagues [7] demonstrated that one year of passive myofunctional therapy in children with OSA produced significant reductions in AHI and desaturation events, along with greater mandibular growth (Co–Gn, N–Me) and increased oropharyngeal airway width (OPha–Ophp), accompanied by improvements in multiple OSA-18 quality-of-life domains. Complementing these findings, Guilleminault et al. [8] showed that children who did not receive myofunctional re-education after adenotonsillectomy frequently experienced recurrence of sleep-disordered breathing, whereas those who completed therapy maintained normal polysomnographic outcomes, underscoring the long-term importance of orofacial muscle function in airway stability. Li et al. [9] similarly found that adenoid hypertrophy leads to vertical craniofacial growth patterns, mandibular retrognathia, elevated nasal airway resistance (5.11 ± 1.95 cmH_2O/L·min), and reduced nasopharyngeal volume (16.86 ± 3.93 cm^3), concluding that AH-induced obstruction alters naso-oropharyngeal dimensions, impairs respiratory function, and contributes to upper-airway stenosis and growth disturbances.

Developmental studies have clarified how the pediatric airway evolves structurally. Chuang et al. [10] investigated upper-airway development from birth to age 5 and found that growth is greatest in the vertical and transverse dimensions, with the lumen becoming increasingly elliptical. They observed early sex-related differences, including larger pharyngeal measurements in females and subglottic differences pre-puberty, concluding that 3D imaging is essential for accurately characterizing these developmental changes. Methodological work by Aboudara et al. [11] showed that CT-derived airway volumes exhibit greater intra-subject variability than cephalometric airway areas, indicating that 2D films only moderately represent true 3D airway morphology. Jacob and Buschang [12] further contributed longitudinal evidence showing that vertical facial proportions and mandibular plane angles change significantly during adolescence, with many individuals maintaining their vertical growth tendencies over time—information that contextualizes the developmental stability of craniofacial patterns associated with airway function.

Sinonasal development also plays a critical role in shaping pediatric airway function. According to Ahmed [13] sinus development in children is dynamic, requiring imaging approaches capable of

 doi:10.20944/preprints202605.1331.v1

capturing complex congenital, inflammatory, traumatic, and neoplastic variations. Lee et al. [14] similarly noted that pediatric paranasal sinuses undergo complex, age-dependent development across the maxillary, frontal, ethmoid, and sphenoid regions, and that conditions such as cystic fibrosis, chronic sinusitis, deviated septum, and cleft lip/palate can alter sinus growth and morphology. They emphasized that although FESS is increasingly used in children, evidence regarding its effects on facial growth and postoperative symmetry remains limited.

The clinical burden of pediatric sinonasal disease further illustrates how inflammation and obstruction influence craniofacial and airway development. Stenner and Rudack [15] described how pediatric nasal and sinus diseases span numerous inflammatory and developmental conditions, with allergic rhinitis—affecting 40% of children in Western Europe—capable of disturbing midfacial growth. Badr et al. [16] reported that pediatric chronic rhinosinusitis involves persistent sinonasal inflammation lasting >3 months, often mimicking allergic rhinitis and adenoid hypertrophy, and emphasized that treatment is primarily medical. Quintanilla-Dieck and Lam [17] highlighted the diagnostic challenges and limited evidence base for pediatric CRS management, noting that adenoidectomy remains central while balloon sinuplasty and FESS benefit selected cases. Fokkens et al. [18] provided updated EPOS2020 recommendations, including revised definitions, a new CRS classification system, and integrated care pathways, while identifying persistent knowledge gaps.

Finally, Fagundes et al. [19] conducted a systematic review and meta-analysis evaluating craniofacial features in children with OSA, reporting that although some studies identified mandibular retrognathia, reduced nasopharyngeal dimensions, and narrower intercanine width, overall evidence remains inconsistent, with meta-analysis showing no significant differences in key cephalometric angles—highlighting the complexity and heterogeneity of craniofacial–airway relationships. Very recently, Bulut et al. [20] identified that global research on pediatric craniofacial growth and airway physiology—based on 1214 publications—has expanded, with major thematic clusters spanning airway function/OSA, craniofacial growth, congenital anomalies, surgical adaptation, and 3D imaging. They noted a shift from broad anatomical studies toward clinically focused, disease-specific topics between 2020–2024 and concluded that contemporary work increasingly integrates dentofacial development with respiratory physiology, underscoring the need for interdisciplinary frameworks in pediatric airway management.

1.2. Airway Biomechanics, Aerodynamics & Mucus Physiology

The human airway system relies on a highly coordinated biomechanical and aerodynamic apparatus to maintain pulmonary sterility and ensure efficient gas exchange. Central to this defense is the mucus clearance system, which constitutes the dominant mechanical host-defense mechanism of the lung [21,22]. Each day, the airways are exposed to an estimated 10^6–10^{10} inhaled bacteria and particulates [23], requiring a robust, dynamic, and responsive clearance mechanism. Traditionally, mucociliary clearance (MCC) was conceptualized as the movement of a mucus gel layer over a watery periciliary "sol" layer [24]. However, this model failed to explain key biomechanical observations, including why mucins do not penetrate interciliary spaces and how the mucus layer remains mechanically coupled to cilia under varying hydration states.

Recent advances have reframed airway mucus physiology through the gel-on-brush model, which incorporates the role of tethered mucins forming a dense periciliary glycocalyx [25].This model provides a more accurate biomechanical explanation for mucus–cilia interactions, osmotic coupling, and the hydration-dependent modulation of mucus transport.

Mucus transport must be understood across multiple length scales, from lung-wide airflow dynamics to microscopic polymer interactions. The lung's small airways collectively provide a surface area of ~1–2 m^2, funnelling mucus toward the third-generation bronchi, where the surface area narrows dramatically to ~50 cm^2 [26]. This anatomical "choke point" creates a biomechanical gradient that facilitates proximal mucus movement.

At the macroscopic level, airflow contributes to mucus propulsion through two-phase gas–liquid pumping and cough-dependent mechanisms [27]. These aerodynamic forces interact with

 doi:10.20944/preprints202605.1331.v1

mucus rheology, which is strongly dependent on mucin concentration. The gel-on-brush model accurately predicts mucus transport rates based on the relative osmotic moduli of the mucus layer and the periciliary layer glycocalyx [25,28]. When mucus becomes hyperconcentrated, its osmotic modulus increases, generating compressive forces that collapse the periciliary layer and impair ciliary beating.

Two high-molecular-weight mucins dominate airway mucus: MUC5B and MUC5AC [29–32].Their secretion patterns are regionally specialized. In healthy lungs, CCSP1⁺ club cells in both proximal and distal airways constitutively secrete MUC5B via a small-granule pathway (~100 nm) [33,34]. Submucosal glands (SMGs) supplement this secretion, particularly during cough reflex activation [35,36]. Because distal airways possess a vastly larger surface area, they contribute the majority of MUC5B under basal conditions.

In contrast, MUC5AC is minimally expressed in healthy airways [37,38] but is strongly induced under pathological stress, including inflammation, infection, and epithelial injury [32,39–41]. This induction involves metaplasia of club cells into goblet cells, which accumulate large mucin granules (~1 μm) [37]. The regulation of MUC5AC secretion differs fundamntally from the constitutive MUC5B pathway, relying on Ca^{2+}-dependent GPCR signaling [32,38].

Normal airway mucus is a hydrogel composed of ~97.5% water, 0.9% salt, ~1.1% globular proteins, and ~0.5% mucin polymers [29]. Hydration status is traditionally measured as percent solids (%TS) [42,43], but more accurate biophysical characterization uses organic percent solids (%OS) and absolute mucin concentration [42,44].

Mucin polymers are extraordinarily large (2.5 MDa per macromonomer) and heavily glycosylated (~75% carbohydrate mass) [27,45]. Their glycan side chains provide hydration sites, negative charge, and low-affinity binding interactions with inhaled particles [23,46,47]. Mucus viscoelasticity, osmotic modulus, and adhesive/cohesive forces scale as high-order powers of mucin concentration [25,28,48]. Even small increases in concentration produce dramatic increases in viscosity.

Therefore, the geometric structural changes induced by orthopedic treatment inevitably alter the intranasal aerodynamics, which directly influences the mucociliary transport efficiency and the apparent rheology of the mucus layer described above.

1.3. Orthopedic Modulation of Airway Structure

Orthopedic modulation of the craniofacial complex has long been recognized as a central mechanism for altering upper airway structure, with early clinical observations gradually evolving into sophisticated biomechanical and aerodynamic analyses. Because the maxilla forms the inferior boundary of the nasal cavity and contributes to the lateral nasal walls and anterior nasopharyngeal framework, orthopedic forces applied to this region inevitably influence sinonasal geometry and airflow behavior. Over the past six decades, research has progressed from foundational clinical descriptions of rapid maxillary expansion (RME) to advanced finite element method (FEM), cone-beam computed tomography (CBCT), and computational fluid dynamics (CFD), each contributing to a more complete understanding of how orthopedic interventions reshape the airway.

The earliest evidence linking maxillary expansion to airway improvement emerged from clinical work in the 1960s and 1970s. Haas [49] demonstrated that opening the mid-palatal suture increased nasal cavity volume and improved nasal breathing, establishing the foundational concept that maxillary expansion has airway benefits. Hicks [50] later showed that slow maxillary expansion in younger patients produced more skeletal and less dental response, reinforcing the importance of early intervention and suggesting that skeletal changes, rather than dental tipping, were responsible for airway improvements. These early clinical insights set the stage for later biomechanical investigations.

The early 2000s marked a transition toward computational modeling, which provided the first quantitative insights into how orthopedic forces propagate through craniofacial structures. Jafari et al. [51] conducted one of the first three-dimensional FEM studies of RME, demonstrating forward

 doi:10.20944/preprints202605.1331.v1

displacement of the nasal septum and downward displacement of midline structures. These findings provided a mechanical explanation for the nasal airway improvements observed clinically. Gautam et al. [52] expanded on this work by mapping stress distribution across circummaxillary sutures, identifying the frontomaxillary, nasomaxillary, and frontonasal sutures as regions of maximal stress during expansion. Their findings confirmed that orthopedic forces extend beyond the palate and influence the nasal framework. Priyadarshini et al. [53] further demonstrated that RME produces pyramidal maxillary displacement, with widening greatest at the nasal floor, directly supporting the concept that expansion modifies airway geometry.

As imaging technology advanced, CBCT studies in the 2010s provided volumetric confirmation of these biomechanical predictions. These studies consistently showed increases in nasal cavity volume, nasopharyngeal space, and total airway dimensions following expansion. Lo Giudice et al. [54] provided one of the most comprehensive CBCT-CFD analyses to date, demonstrating that the maxilla "constitutes the lower border of the nasal cavity," and that opening the mid-palatal suture simultaneously enlarges the nasal cavity laterally. Their CFD results showed significant reductions in airflow pressure and velocity 12 months after RME, with the early expansion group exhibiting a 33.65% reduction in pressure and a 34.24% reduction in velocity. These findings confirmed that expansion not only alters skeletal boundaries but also improves aerodynamic efficiency.

Parallel to these developments, research into skeletal anchorage systems refined the understanding of how different expansion modalities influence airway structure. MARPE emerged as a technique capable of producing more skeletal and less dentoalveolar expansion. MacGinnis et al. [55] demonstrated via FEM that MARPE directs tension and compression to the palate and reduces unwanted maxillary rotation, producing a more parallel expansion pattern. Lee and colleagues [56] showed that micro-implant placement on the palatal slopes minimized stress concentration and dental tipping, confirming that bone-borne expanders generate more uniform stress distribution across the palate. These findings established MARPE as a superior method for achieving skeletal expansion in adolescents and adults, with direct implications for airway improvement.

The refinement of FEM methodology also depended on accurate material property data. Rees and Jacobsen [57] provided reliable elastic modulus values for the periodontal ligament (PDL), while Ruse [58] highlighted the propagation of erroneous PDL modulus values in FEM literature, emphasizing the need for accurate biomechanical inputs. Vaida et al. [59] contributed data on mechanical properties of orthodontic resins. These studies improved the accuracy of FEM simulations used to model orthopedic airway effects.

As computational methods matured, CFD became a powerful tool for analyzing airflow changes following orthopedic intervention. Attinger et al. [60] provided methodological insights into fluid dynamics modeling, supporting the CFD approaches used in airway studies. The CFD simulations have been developed over the past two decades. Recentely, Lo Giudice et al. [54] applied CFD to quantify airflow changes after RME, demonstrating that expansion reduces negative pressure zones and peak airflow velocity, both of which are associated with airway obstruction. Their study also showed that nasopharyngeal volume increased by 70.33% in the early expansion group and 23.57% in the late expansion group, highlighting age-dependent differences in skeletal responsiveness.

Age remains a critical factor in orthopedic airway modulation. As early as 1978 Hicks [50] demonstrated that younger patients exhibit more skeletal expansion and less dental tipping. Year later, Boryor et al. [61] showed that adult expansion produces linear strain behavior until rupture, highlighting the biomechanical limitations of mature sutures and explaining why airway improvements are more pronounced in younger individuals. Similarly, Angelieri et al. [62] and very recently Lo Giudice et al. [54] mentioned that younger patients experienced greater airway improvements, consistent with the sutural maturation stages.

Orthopedic modulation of airway structure is not purely skeletal and improvements in airflow were partly due to spontaneous regression of adenotonsillar tissue, suggesting that skeletal expansion may create a more favorable biomechanical environment for soft-tissue remodeling. Tanaka et al. [63,64] demonstrated that orthopedic forces alter periodontal ligament stress patterns,

 doi:10.20944/preprints202605.1331.v1

indicating that soft-tissue structures adapt alongside skeletal changes. Also, it has been highlighted that nasomaxillary expansion improves nasal airflow and reduces pharyngeal collapsibility, and that craniofacial manipulations influence lymphatic drainage and autonomic regulation.

Collectively, these findings demonstrate that orthopedic interventions—RME, MARPE, and sRME—modulate airway structure through lateral expansion of the nasal cavity, increased nasopharyngeal volume, reduced airflow resistance, sutural remodeling, and secondary soft-tissue changes. Chronologically, the field has progressed from early clinical observations to sophisticated biomechanical and aerodynamic analyses, each layer of evidence reinforcing the conclusion that maxillary expansion plays a significant role in optimizing upper airway structure and function.

1.4. RAMPA Superiority in Orthopedic Maxillary Protraction

Conventional orthodontic and orthopedic interventions for maxillary hypoplasia—including rapid maxillary expansion (RME), slow maxillary expansion (SME), semi-rapid maxillary expansion (sRME), facemask protraction, chin-cup therapy, and headgear—have been widely used for over a century. However, despite their historical prevalence, a substantial body of evidence demonstrates that these modalities exhibit biomechanical limitations, inconsistent skeletal effects, undesirable vertical side-effects, and inadequate control of maxillary rotational vectors. Consequently, these shortcomings have motivated the development of more physiologically coherent systems. By mimicking the natural anterosuperior growth trajectory of the maxillopalatal complex, the Right Angle Maxillary Protraction Appliance (RAMPA) delivers a physiologically aligned, controlled, multi-vector force. Recent finite element method (FEM) studies and clinical investigations have confirmed that RAMPA overcomes the limitations of conventional therapies, aligning with both craniofacial growth trajectories and sinonasal physiology [64].

RAMPA system addresses theaforementioned limitations through a unique force vector that consistently produces forward-and-upward maxillary displacement. Finite element method studies demonstrate that RAMPA elevates the center of rotation and increases the radius of maxillary rotation, generating expansion that is more parallel to the palatal plane [1]. FEM analysis revealed an increased radius and elevated center of maxillary rotation, producing expansion that was more parallel to the palatal plane. This contrasts sharply with the posteroinferior displacement commonly associated with facemask therapy. Additional FEM simulations confirm that RAMPA rotates both the maxilla and mandible in the forward direction, producing anterosuperior protraction even under varying suture stiffness conditions [66–68].

Clinical evidence further reinforces RAMPA's superiority. CBCT-based volumetric studies show that RAMPA produces sinonasal expansion exceeding natural growth rates. One cohort demonstrated a 16.24% increase in total sinonasal volume over approximately eight months, with an annualized growth velocity 120% greater than physiological norms [69]. Another comparative study found that children with baseline sinus opacification experienced a 61% increase in airway volume—far greater than the 18% increase observed in clear-sinus patients—indicating both skeletal remodeling and rapid obstruction relief [70]. These findings align with the clinical observation that nasal passages widened, paranasal opacities resolved, and occlusal and intermolar widths improved [71]. Via two-phase air–mucus simulations the previous research also demonstrate that nasal cavity expansion under RAMPA increases airflow velocity and pressure drop, enhancing the suction effect responsible for frontal sinus mucus clearance [71]. Furthermore, RAMPA avoids the limitations of RME-based systems, which often produce non-parallel expansion and limited forward displacement. When combined with intraoral devices such as gHu-1 or VomPress, RAMPA maintains lateral expansion while simultaneously achieving controlled anterosuperior protraction—an effect repeatedly confirmed across FEM, cephalometric, and clinical studies [66–68,72].

Collectively, the evidence demonstrates that RAMPA surpasses existing orthodontic methods by delivering predictable anterosuperior maxillary advancement, superior sinonasal volumetric gains, improved mucus clearance, and consistent airway enhancement. Its integrated biomechanical

 doi:10.20944/preprints202605.1331.v1

and aerodynamic validation positions RAMPA as the most comprehensive and physiologically aligned orthopedic therapy currently available.

In this feature paper, we provide a comprehensive review that integrates nearly a decade of interdisciplinary research, ranging from foundational bone physiology to advanced computational modeling (FEM and CFD) and clinical longitudinal studies. Our objective is to establish a cohesive scientific framework that elucidates how RAMPA therapy optimizes craniofacial harmony, sinonasal geometry, and respiratory function, thereby positioning it as a physiologically aligned paradigm in pediatric airway management.

2. Description of the RAMPA System and Mechanotherapy Principle

To realize the theoretical anterosuperior force vector required to stimulate physiological circummaxillary suture growth, the RAMPA system utilizes a specialized, extraoral framework combined with patient-specific intraoral appliances. Figure 1 provides a comprehensive overview of the physical components and the therapeutic setup.

The extraoral component, RAMPA (Figure 1A), is a robust, rigid metallic structure engineered to establish a stable reference frame relative to the calvaria. The functional hallmark of this extraoral unit is its customizable force delivery system, designed to exert vectors at precise perpendicular or obtuse angles relative to the occlusal plane. The intraoral appliance consists of acrylic resin and the screw for activation as shown in Figure 1B. It is connected to the bow for RAMPA System configuration and applied to patients as shown in Figure 1C. The applied forces from rubber bands in RAMPA, i.e., the horizontal force F1, the front-vertical force F2, and the rear force F3, are shown in Figure 1A. Each force is applied symmetrically to both sides with respect to the center line of the nose.

The strategic integration of these specific force components (F1, F2, and F3) is engineered to synthesize a net biomechanical vector that fundamentally differs from conventional orthopedic treatments. Figure 2 conceptually illustrates this biomechanical synergy and its clinical implications. While traditional facemask therapy (Figure 2A) typically applies an anteroinferior force that inadvertently induces an undesirable clockwise rotational moment (M) of the mandible and a downward tipping of the maxilla, the Right Angle Maxillary Protraction Appliance (RAMPA) therapy circumvents these side effects. As depicted in Figure 2B, the RAMPA system utilizes its rigidly anchored extraoral frame to convert the individualized elastic forces into a dominant, net anterosuperior protraction vector (F). This precise vector control generates a counterclockwise rotational moment (M), providing an anti-gravitational lift to the entire maxillomandibular complex. By directing forces anterosuperiorly, this mechanotherapy activey stimulates the frontomaxillary and circummaxillary sutures, guiding true three-dimensional biomimetic structural remodeling rather than mere downward displacement.

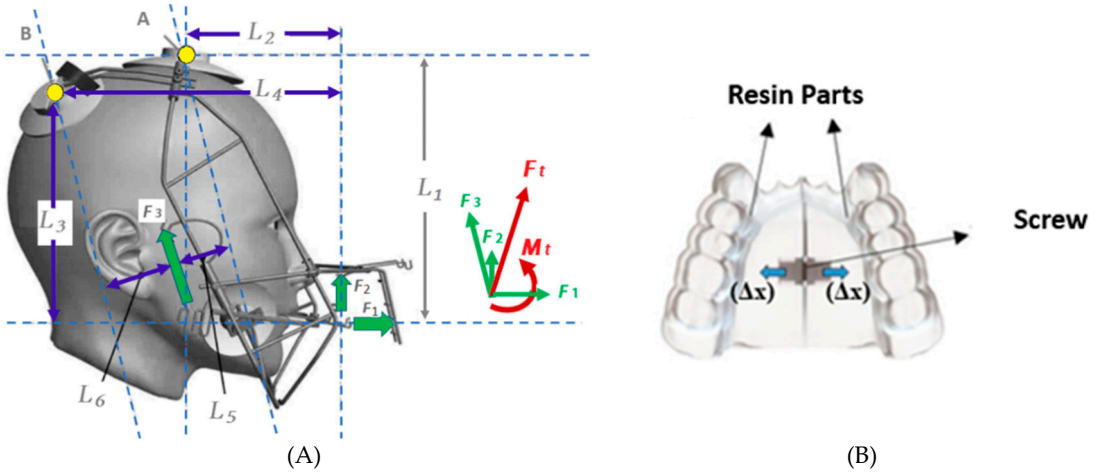

(A) (B)

 doi:10.20944/preprints202605.1331.v1

(C)

Figure 1. Overview of the RAMPA appliance system and mechanotherapy setup; (A) Extraoral device, RAMPA, (B) Intraoral device, (C) Intraoral device connected with bow.

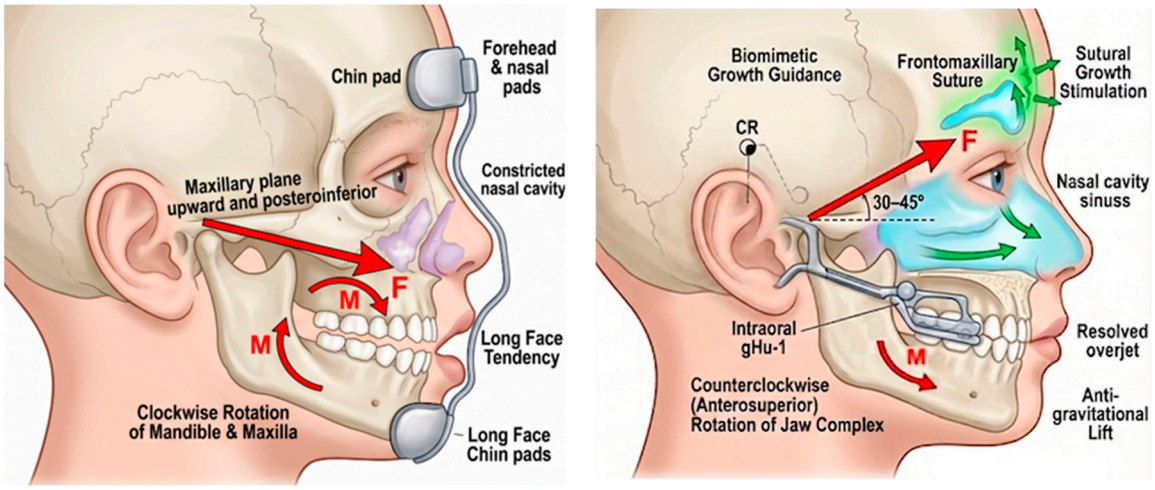

(A) (B)

Figure 2. Conceptual Diagram of RAMPA Therapy's Biomimetic Approach and Comparison to Conventional Facemask; (A) Conventional Facemask Therapy, (B) RAMPA Therapy.

3. Biomechanical Foundations: Finite Element Modeling (FEM)

The fundamental efficacy of RAMPA therapy lies in its ability to modulate mechanical stress across the craniofacial sutures. A series of high-fidelity FEM investigations have successfully quantified these biomechanical interactions.

3.1. Anterosuperior Protraction and Center of Rotation

Traditional maxillary protraction frequently forces the maxilla to move in a downward and forward trajectory. FEM analyses have demonstrated that the RAMPA extraoral appliance effectively acts against gravity. When subjected to anterosuperior force vectors, RAMPA shifts the center of rotation toward the superior-posterior cranial base. This shift translates into a forward and upward bodily movement of the maxillopalatal complex, minimizing the downward tipping of the palatal plane and preventing the typical clockwise rotation of the mandible. These biomechanical dynamics are visually confirmed in Figure 3. The FEM simulation (Figure 3A) explicitly maps the anterosuperior displacement vectors across the maxilla. Crucially, this theoretical model is validated by clinical evidence; 3D CT superimpositions (Figure 3B) over a 17-month treatment period demonstrate a true skeletal translation that mirrors the predicted anterosuperior growth pattern.

 doi:10.20944/preprints202605.1331.v1

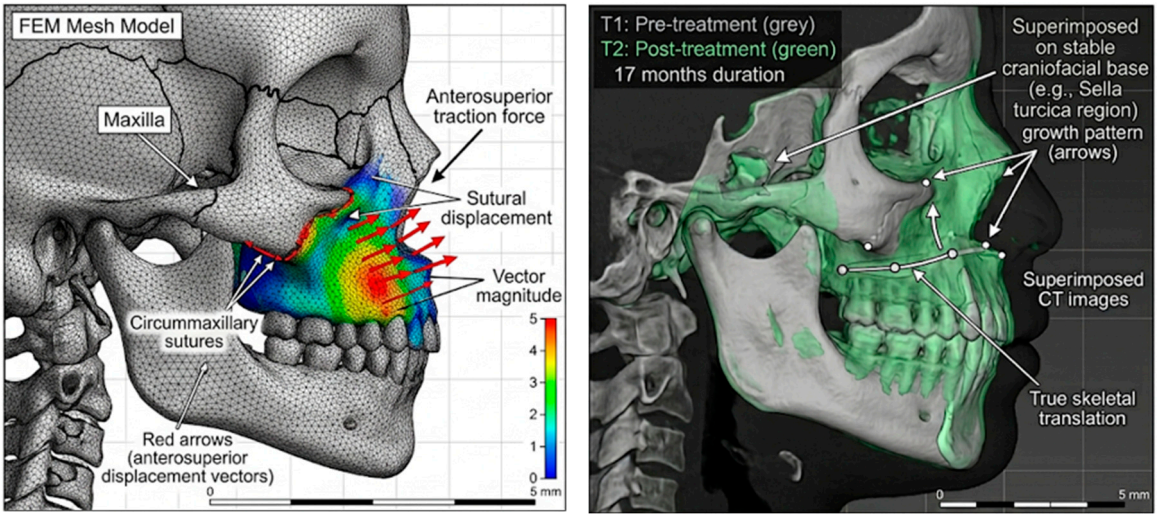

(A) (B)

Figure 3. Comparison of FEM simulation results and clinical case of anterosuperior maxilla displacement by RAMPA appliance. (A) FEM Simulation: Visualizes the anterosuperior displacement vectors (red arrows) and displacement contours appearing on the maxilla during RAMPA appliance wear. Displacement magnitude increases as the color progresses from blue (low displacement) to red (high displacement). (B) Clinical Case: Superimposes 3D CT images of the same patient before treatment (T1, grey) and after 17 months of treatment (T2, green), confirming the same anterosuperior growth pattern as the simulation at the actual skeletal level.

3.2. Synergies with Intraoral Appliances

The integration of RAMPA with specific intraoral devices—such as the gHu-1, VomPress, and Hybrid appliances (summarized in Table 1)—further refines this displacement. Simulations of RAMPA combined with the gHu-1 semi-rapid maxillary expansion (sRME) device proved that the extraoral upward pull does not interfere with the lateral expansion generated by the intraoral screw. Instead, it transforms mid-palatal suture displacement from a slight postero-inferior drift into a definitive anterosuperior lift. Furthermore, combinations with the VomPress and novel Hybrid intraoral appliances have shown profound clinical advantages. Both FEA and supporting clinical case reports of growing patients (e.g., a 7-year-old female treated over 17 months) revealed that the Hybrid/RAMPA combination successfully induced a counterclockwise mandibular rotation (-1.0 degree) and a decrease in the RAMUS angle (2.9 degrees), successfully mitigating long-face tendencies and improving overall facial profile and cervical posture.

Table 1. Summary of primary intraoral appliances used with RAMPA.

Intraoral Appliance	Design & Characteristics	Key Biomechanical & Clinical Effects with RAMPA
gHu-1 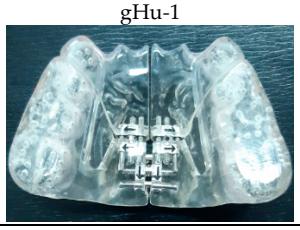	Semi-rapid maxillary expansion (sRME) device: Guides progressive lateral expansion of the palatal suture via screw activation.	• Simultaneous expansion without interference: Anterosuperior protraction force of RAMPA and lateral expansion occur simultaneously without mechanical interference. • Transformation of displacement vector: Transforms subtle postero-inferior displacement that may occur in the mid-palatal suture region into distinct anterosuperior lifting (FEM verified).
VomPress 	Space-creating appliance: Designed to physically expand intraoral volume to secure initial space for tongue positioning and airway.	• Correction of cervical posture: As the airway opens through anterosuperior traction of the maxilla and securing space, it clinically induces distinct improvement in Straight Neck Problem and overall cervical posture. • Effective improvement of anterior overjet and malocclusion.

 doi:10.20944/preprints202605.1331.v1

Hybrid	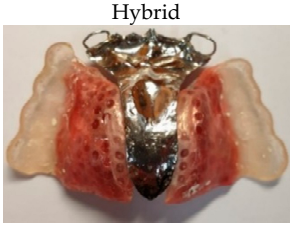	Novel Hybrid appliance (Multi-control type): Latest model combining advantages of existing devices to control three-dimensional movement of the maxilla more precisely.	• Control of mandibular rotation: Induces counterclockwise rotation (-1.0 degree) and decrease in RAMUS angle (2.9 degrees) of the mandible to effectively alleviate Long-face Syndrome. • Maximization of anterosuperior rotation: Demonstrates a synergistic effect maximizing anterosuperior rotation of the maxilla complex while minimizing downward displacement of the mid-palatal suture.

3.3. Predictability Across Suture Maturation

Because biological tissue properties vary by age and individual, the impact of suture stiffness (Young's modulus) on treatment outcomes is a critical clinical variable. FEM simulations testing varied sutural moduli (30, 50, and 80 MPa) against RAMPA forces showed that structural displacement and von Mises stresses possess a predictable, linear relationship with suture stiffness. Unlike rigid models that exhibit erratic stress concentrations, flexible physiological suture models demonstrate that RAMPA maintains its effective anterosuperior protraction pattern across a broad spectrum of tissue elasticities, affirming its applicability across different pediatric developmental stages.

3.4. Mechanotransduction and Osteogenic Signaling

Beyond macroscopic skeletal displacement, the therapeutic efficacy of the RAMPA system is anchored in the principles of cellular mechanotransduction. Recent finite element analyses have specifically identified regions across the circummaxillary sutures where anterosuperior force vectors concentrate tensile stress, defining a "BMP-2 Trigger Zone" (Figure 4A). In these highly stressed regions, mechanical strain reaches the biological thresholds necessary to induce osteogenic signaling and the upregulation of Bone Morphogenetic Protein-2 (BMP-2), as conceptualized in the mechanotherapeutic pathway (Figure 4B). This demonstrates that RAMPA acts not merely as a physical expander, but as a mechanotherapeutic modulator that triggers molecular signaling for active bone formation and remodeling at the sutural microenvironment.

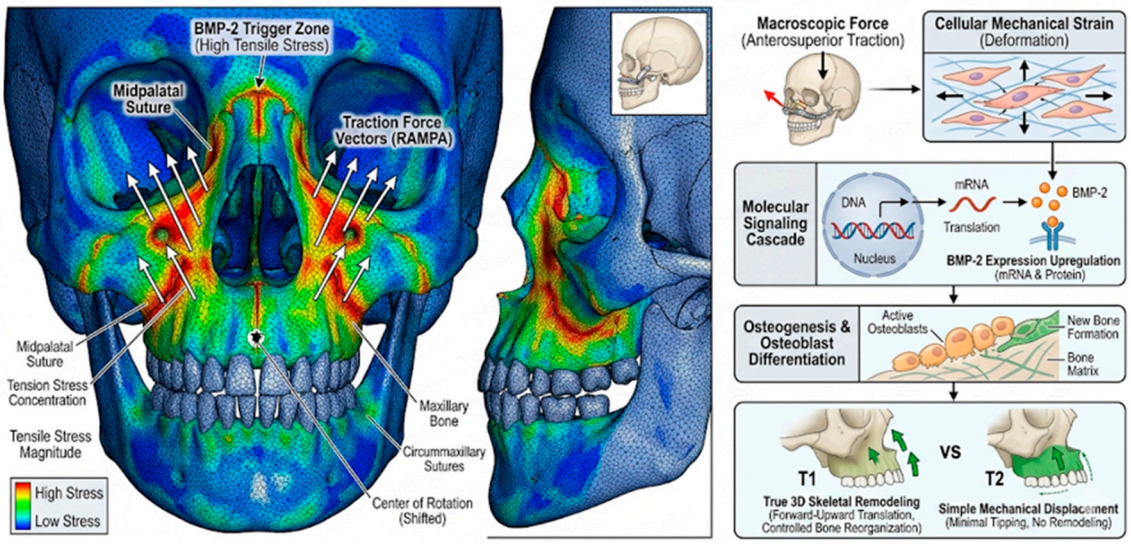

(A) (B)

Figure 4. Mechanotransduction pathway and identification of the "BMP-2 Trigger Zone" during Right Angle Maxillary Protraction Appliance (RAMPA) therapy. (A) FEM Stress Distribution Map: Finite element analysis illustrating the concentration of tensile stress across the circummaxillary and midpalatal sutures. The highly stressed areas (warm colors) define the 'BMP-2 Trigger Zone,' where mechanical strain reaches physiological thresholds. (B) Biological Cascade Schematic: A conceptual representation of the mechanotherapeutic pathway. The macroscopic anterosuperior orthopedic forces are transduced into cellular mechanical strain, which actively

 doi:10.20944/preprints202605.1331.v1

upregulates Bone Morphogenetic Protein-2 (BMP-2) expression, thereby initiating molecular osteogenesis and true three-dimensional skeletal remodeling rather than simple mechanical displacement.

4. Aerodynamic Reconfiguration and Fluid Mechanics (CFD)

The orthopedic expansion of the maxilla directly alters the internal geometry of the nasal airway. To understand how these skeletal changes restore respiratory function, advanced Computational Fluid Dynamics (CFD), particularly two-phase air-mucus volume of fluid (VOF) simulations, have been employed.

4.1. Reduction of Airflow Resistance

CFD models reconstructed from patient CBCT data reveal that the RAMPA-induced widening of the nasal passages drastically alters internal aerodynamics. An expanded nasal cavity increases the cross-sectional area, reducing overall airflow resistance and eliminating turbulent, stagnant airflow zones. The resulting acceleration in airflow velocity across the superior nasal meatus ensures that ventilation reaches the critical ostial pathways connecting the paranasal sinuses.

4.2. Two-Phase Fluid Dynamics and Mucus Clearance

Impaired mucus drainage is the primary pathophysiological driver of chronic rhinosinusitis and pediatric empyema. Using unsteady RANS turbulence models and non-Newtonian shear-thinning frameworks, two-phase CFD analyses have mapped the interaction between accelerated airflow and viscous mucus (Figure 5). The simulations demonstrated that the structural expansion achieved via RAMPA+sRME (Figure 5A) significantly enhances the "suction effect" near the sinus ostia (Figure 5B). This aerodynamic shift physically drives mucus expulsion from the maxillary and frontal sinuses, proving that RAMPA acts as a mechanotherapeutic trigger that resolves mucostasis without the need for surgical or primary pharmacological intervention.

Furthermore, to accurately capture the complex behavior of respiratory mucus, recent CFD simulations have successfully employed the Carreau-Yasuda rheological framework. These advanced two-phase air-mucus models demonstrate that the structural expansion achieved by RAMPA therapy significantly reduces wall shear stress (WSS) and improves overall airflow distribution. This optimized aerodynamics provides the critical physical conditions necessary to facilitate the transition of mucus from a stagnant, high-viscosity state to a mobilizable fluid state via shear-thinning effects. Consequently, this aerodynamic reconfiguration physically drives mucus expulsion from the sinuses (Figure 5C), proving that RAMPA resolves mucostasis through sophisticated fluid-structure interactions.

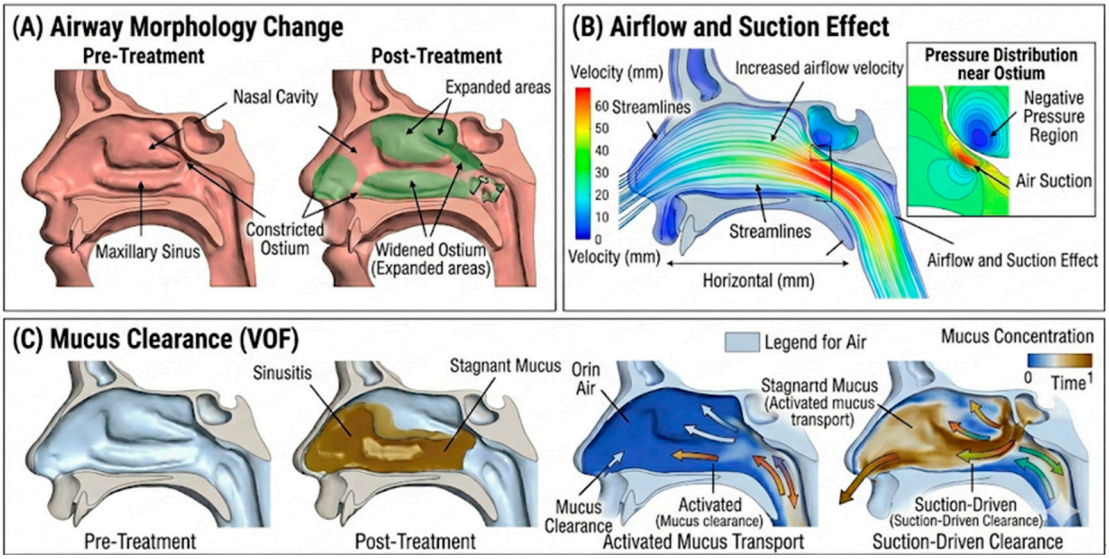

 doi:10.20944/preprints202605.1331.v1

Figure 5. The Impact of Right Angle Maxillary Protraction Appliance (RAMPA) Therapy on Nasal Cavity and Sinus Aerodynamics and Mucus Clearance. (A) Airway Morphology Change: A comparison of sagittal skull models showing pre-treatment constricted nasal cavity and sinuses, and post-treatment expanded areas (highlighted in transparent green). (B) Airflow and Suction Effect: Visualization of improved aerodynamics using post-treatment geometry. Colored streamlines indicate expanded airway flow and increased airflow velocity, while the pressure distribution inset illustrates the formation of a negative pressure region near the ostium, resulting in an air suction effect into the sinus. (C) Mucus Clearance (VOF): Conceptual snapshots from a VOF-based two-phase flow simulation over conceptual time. The top rows represent a sinusitis condition with stagnant mucus within a constricted sinus. The bottom rows demonstrate how the newly developed negative conceptual pressure mobilizes the conceptual cluster, facilitating mucus clearance from the maxillary sinus into the nasal cavity via suction-driven clearance.

5. Clinical Outcomes and Volumetric Tracking

The translation of these computational predictions into clinical reality has been validated through large-cohort retrospective studies utilizing both traditional cephalometrics (Coben analysis) and advanced 3D CBCT volumetry.

5.1. Skeletal Growth and Coben Analysis

In a cohort of 30 growing patients, Coben analysis revealed statistically significant improvements in facial depth (Ba-N) and anterior facial height (N-Me) for both sexes following RAMPA therapy (Figure 6A,B). Crucially, the treatment induced favorable mandibular adaptation: male patients exhibited an average 1.47° decrease in the Gonial Angle (indicative of anterior rotation) (Figure 6C), while female patients demonstrated a significant increase in the maxillary depth ratio. These findings confirm the system's capacity to restore 3D craniofacial balance in skeletal Class III profiles.

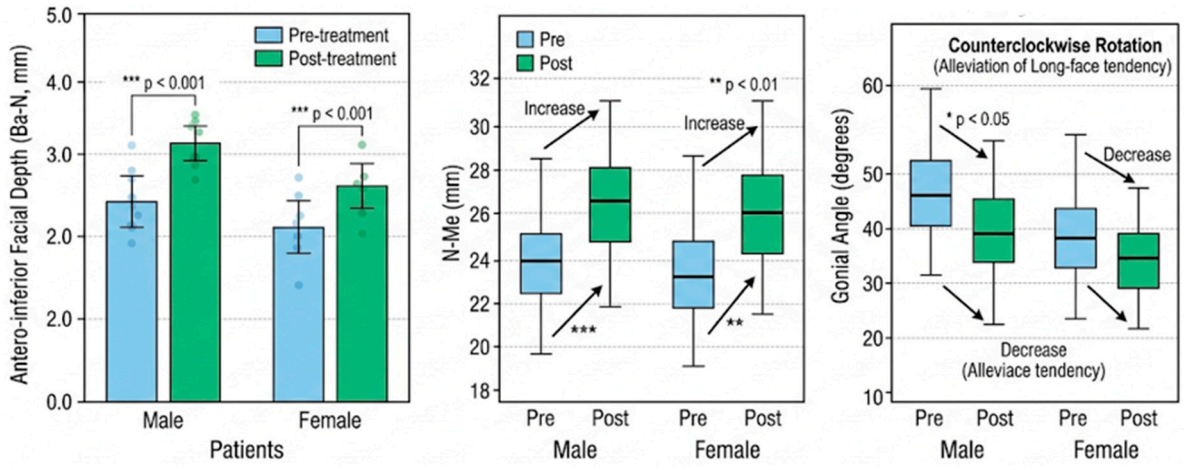

Figure 6. Statistical analysis of changes in facial skeletal morphology following Right Angle Maxillary Protraction Appliance (RAMPA) therapy using Coben analysis (n=30). (A) Facial Depth (Ba-N, mm): Demonstrates a significant increase in post-treatment values across both male and female cohorts ($p < 0.001$). (B) Anterior Facial Height (N-Me, mm): Visualizes significant increases in N-Me values for both sexes ($p < 0.01$, $p < 0.001$), indicating controlled vertical growth. (C) Mandibular Angle (Gonial Angle, degrees): Reveals a significant decrease ($p < 0.05$) and counterclockwise rotation, specifically in the male cohort; the female group shows a downward trend with lower statistical significance.

5.2. Accelerated Sinonasal Volumetric Expansion

A volumetric analysis of the complete sinonasal complex (nasal cavity and all four paranasal sinuses) in 60 pediatric patients demonstrated a massive 16.24% mean volume gain over an average

 doi:10.20944/preprints202605.1331.v1

treatment period of just 8.38 months. Strikingly, the annualized volumetric growth velocity achieved under RAMPA therapy outpaced the natural physiological growth baselines (age-matched normative data) by a factor of 1.2 (Figure 7B). This rapid "catch-up" growth trajectory (Figure 7A) proves that RAMPA provides an active acceleration effect, physically remodeling the respiratory environment faster than natural maturation.

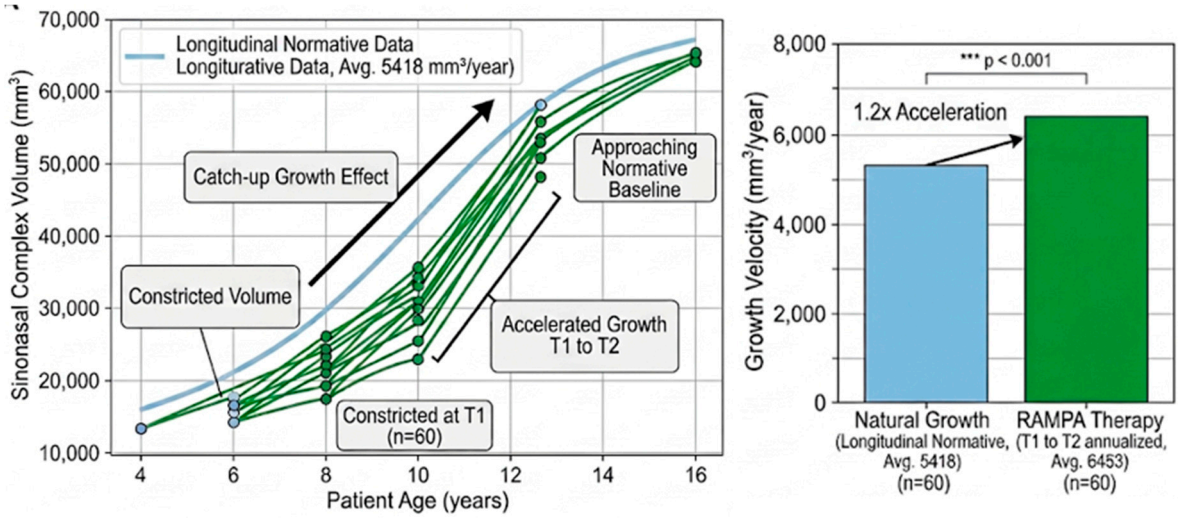

(A) (B)

Figure 7. Volumetric growth velocity comparison of the sinonasal complex: Natural growth versus Right Angle Maxillary Protraction Appliance (RAMPA) therapy (n=60). (A) Volumetric Growth Trajectory: Illustrates changes in sinonasal complex volume relative to patient age. Patients beginning treatment with pathologically constricted volumes (below the light-blue longitudinal normative baseline) exhibit a rapid "catch-up" growth trajectory (steep green lines) that converges toward normal levels. (B) Annual Volumetric Growth Velocity Comparison: A quantitative bar chart demonstrating that the annualized growth velocity under RAMPA therapy (avg. 6453 mm³/year) is significantly faster than the natural growth baseline (avg. 5418 mm³/year), achieving a 1.2-fold acceleration effect ($p < 0.001$).

5.3. Differentiated Mechanisms: Clear vs. Opacified Sinuses

The most profound clinical validation of RAMPA's mechanotherapeutic effects stems from a comparative study differentiating patients based on baseline sinonasal health: those with clear paranasal sinuses (n=26) versus those with pre-existing opacification or empyema (n=20). While both groups experienced an increase in upper airway volume following RAMPA therapy, the magnitude and underlying mechanisms varied drastically.

- Clear Sinus Group (n=26): Patients exhibited an 18% mean increase in sinonasal volume. Importantly, this increase positively correlated with treatment duration ($r=0.52$, $p<0.05$). This indicates a mechanism of slow-occurring, mechanically driven skeletal adaptation, where steady expansion occurs over time as a direct result of the continuous orthopedic force.
- Opacified Sinus Group (Empyema, n=20): In contrast, patients presenting with chronic sinusitis or empyema demonstrated a staggering 61.2% mean increase in volume ($p<0.0001$). Notably, this massive gain showed no significant correlation with treatment time ($r=0.08$, $p=0.65$). This points to an immediate, duration-independent resolution of soft-tissue obstruction and mucosal edema.

By rapidly resolving chronic mucosal inflammation through improved aerodynamics and restoring sinonasal homeostasis, this evidence confirms that RAMPA therapy functions as a comprehensive mechanotherapeutic solution that goes far beyond simple skeletal expansion. The clinical manifestations of these divergent mechanisms are detailed in Figure 8.

 doi:10.20944/preprints202605.1331.v1

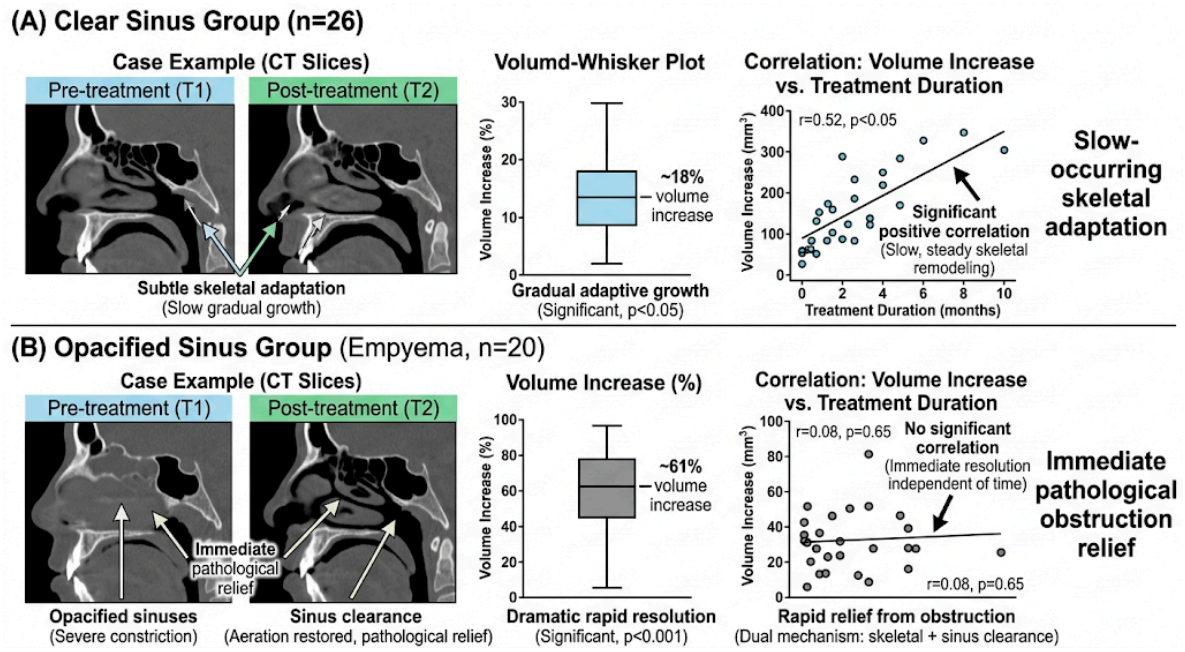

Figure 8. Differential mechanisms of airway expansion following RAMPA therapy based on baseline sinus status. (A) Clear Sinus Group (n=26): Sagittal CT images (Left) show subtle skeletal adaptation. The box plot (Middle) indicates an ~18% volume increase, which strongly correlates with treatment duration (Right), highlighting a slow, steady remodeling process. (B) Opacified Sinus Group (n=20): CT images (Left) demonstrate dramatic clearance of severely opacified sinuses. The box plot (Middle) reveals a massive ~61% volume surge. The lack of correlation with treatment duration (Right) emphasizes an immediate pathological obstruction relief independent of mechanical remodeling time.

6. Discussion

This feature paper systematically synthesizes finite element modeling (FEM), computational fluid dynamics (CFD), and clinical CBCT data to elucidate the multi-disciplinary mechanisms underlying RAMPA therapy. The synthesized evidence demonstrates that RAMPA operates far beyond the boundaries of conventional mechanical expansion; rather, it functions as a comprehensive "mechanotherapeutic modulator." By bridging macroscopic orthopedic forces with microscopic biophysical and molecular responses, this review establishes a clear chain of causality from initial mechanical intervention to the ultimate restoration of sinonasal homeostasis.

6.1. The Mechanotherapeutic Chain of Causality

The foundational mechanism of RAMPA therapy lies in its biomimetic approach to skeletal translation. Conventional therapies often induce rotational side effects that limit true three-dimensional airway expansion. In contrast, FEM studies reviewed herein confirm that RAMPA's anterosuperior force vectors effectively mitigate counterclockwise mandibular rotation while concentrating tensile stress directly across the circummaxillary sutures. Crucially, this targeted stress distribution reaches the mechanical thresholds required to form "BMP-2 Trigger Zones." Within these zones, mechanical strain is transduced into osteogenic signaling, upregulating Bone Morphogenetic Protein-2 (BMP-2) and catalyzing active, molecular-level bone remodeling.

The precise skeletal remodeling initiated by this mechanotransduction profoundly alters the internal fluid dynamics of the sinonasal complex. CFD simulations utilizing the Carreau-Yasuda rheological framework reveal that structural expansion significantly reduces overall airflow resistance while optimizing Wall Shear Stress (WSS) distribution. Because respiratory mucus is a non-Newtonian fluid, the increased airflow velocity and enhanced suction effects generated by the expanded airway exert critical shear forces on stagnant mucus. This triggers a "shear-thinning" effect, causing a dramatic biophysical breakdown in mucus viscosity. Consequently, highly viscous,

 doi:10.20944/preprints202605.1331.v1

trapped mucus becomes fluidized and is actively expelled, proving that RAMPA facilitates functional clearance through sophisticated fluid-structure interactions.

6.2. Clinical Significance of Pathophysiological Resolution

The clinical outcomes from large-cohort longitudinal analyses definitively validate this multi-scale mechanotherapeutic framework. A pivotal finding highlighted in this review is the differential response based on baseline sinonasal health. Patients with pre-existing empyema (opacified sinuses) exhibited a staggering 61.2% volumetric increase, compared to a more gradual 18% increase in patients with clear sinuses. This stark contrast indicates a dual mechanism of action: in healthy airways, RAMPA induces slow-occurring skeletal adaptation; in compromised airways, it provides immediate, duration-independent relief of pathophysiological obstruction and mucosal edema. Furthermore, the overall 1.2-fold acceleration in natural sinonasal growth velocity underscores that RAMPA rapidly drives constricted, pathological anatomies back toward normative developmental baselines.

6.3. Limitations and Future Perspectives

While the integration of computational and clinical data provides a robust mechanistic explanation, future prospective studies are warranted. Direct *in vivo* quantification of molecular markers—such as BMP-2 levels in gingival crevicular fluid or inflammatory cytokines (e.g., TNF-α) in nasal secretions—would further validate the cellular mechanotransduction pathways. Additionally, incorporating patient-specific dynamic CFD models that account for varying degrees of mucosal inflammation will refine our understanding of shear-thinning clearance mechanisms across different pediatric demographics. Lastly, while the massive volumetric gains observed in empyema patients are statistically significant, future studies with matched untreated control groups (though ethically challenging in pediatric populations) would help completely isolate the therapeutic effect from spontaneous resolution.

7. Conclusions

The integration of biomechanical engineering and clinical tracking has firmly established the Right Angle Maxillary Protraction Appliance (RAMPA) as a potent, biomimetic intervention for craniofacial hypoplasia. By maintaining precise anterosuperior force vectors across varying suture stiffness levels, RAMPA circumvents the rotational pitfalls of traditional appliances and actively initiates sutural mechanotransduction, triggering molecular osteogenic signaling for true three-dimensional bone remodeling. More importantly, this highly controlled skeletal remodeling translates directly into optimized internal aerodynamics—reducing airflow resistance, initiating shear-thinning mucus clearance, and yielding massive volumetric airway gains that outpace natural growth. Ultimately, RAMPA therapy transcends traditional dental alignment, offering a holistic mechanotherapeutic cure for pediatric craniofacial and respiratory compromise.

References

1. Moss, M.L.; Salentijn, L. The Primary Role of Functional Matrices in Facial Growth. *Am. J. Orthod.* **1969**, *55*, 566–577, doi:10.1016/0002-9416(69)90034-7.
2. McNamara, J.A. Influence of Respiratory Pattern on Craniofacial Growth. *Angle Orthodontist* **1981**, *51*, 269–300.
3. Solow, B.; Siersbæk-Nielsen, S.; Greve, E. Airway Adequacy, Head Posture, and Craniofacial Morphology. *Am. J. Orthod.* **1984**, *86*, 214–223, doi:10.1016/0002-9416(84)90373-7.
4. Rosetti Lessa, F.C.; Enoki, C.; Neuppmann Feres, M.F.; Pereira Volera, F.C.; Anselmo Lima, W.T.; Nakane Matsumoto, M.A. Breathing Mode Influence on Craniofacial Development. *Revista Brasileira de Otorrinolaringologia* **2005**, *71*, 156–160, doi:10.1590/s0034-72992005000200007.

 doi:10.20944/preprints202605.1331.v1

5. Kim, Y.J.; Hong, J.S.; Hwang, Y.I.; Park, Y.H. Three-Dimensional Analysis of Pharyngeal Airway in Preadolescent Children with Different Anteroposterior Skeletal Patterns. *American Journal of Orthodontics and Dentofacial Orthopedics* **2010**, *137*, 306.e1-306.e11, doi:10.1016/j.ajodo.2009.10.025.
6. Indriksone, I.; Jakobsone, G. The Influence of Craniofacial Morphology on the Upper Airway Dimensions. *Angle Orthodontist* **2015**, *85*, 874–880, doi:10.2319/061014-418.1.
7. Chuang, L.C.; Hwang, Y.J.; Lian, Y.C.; Hervy-Auboiron, M.; Pirelli, P.; Huang, Y.S.; Guilleminault, C. Changes in Craniofacial and Airway Morphology as Well as Quality of Life after Passive Myofunctional Therapy in Children with Obstructive Sleep Apnea: A Comparative Cohort Study. *Sleep and Breathing* **2019**, *23*, 1359–1369, doi:10.1007/s11325-019-01929-w.
8. Guilleminault, C.; Huang, Y.S.; Monteyrol, P.J.; Sato, R.; Quo, S.; Lin, C.H. Critical Role of Myofascial Reeducation in Pediatric Sleep-Disordered Breathing. *Sleep Med.* **2013**, *14*, 518–525, doi:10.1016/j.sleep.2013.01.013.
9. Li, H.; Wang, H.; Hao, H.; An, H.; Geng, H. Influences of Airway Obstruction Caused by Adenoid Hypertrophy on Growth and Development of Craniomaxillofacial Structure and Respiratory Function in Children. *Comput. Math. Methods Med.* **2022**, *2022*, doi:10.1155/2022/5096406.
10. Chuang, Y.J.; Hwang, S.J.; Buhr, K.A.; Miller, C.A.; Avey, G.D.; Story, B.H.; Vorperian, H.K. Anatomic Development of the Upper Airway during the First Five Years of Life: A Three-Dimensional Imaging Study. *PLoS One* **2022**, *17*, doi:10.1371/journal.pone.0264981.
11. Aboudara, C.A.; Hatcher, D.; Nielsen, I.L.; Miller, A. A Three-Dimensional Evaluation of the Upper Airway in Adolescents. *Orthod. Craniofac. Res.* **2003**, *6*, 173–175, doi:10.1034/j.1600-0544.2003.253.x.
12. Jacob, H.B.; Buschang, P.H. Vertical Craniofacial Growth Changes in French-Canadians between 10 and 15 Years of Age. *American Journal of Orthodontics and Dentofacial Orthopedics* **2011**, *139*, 797–805, doi:10.1016/j.ajodo.2010.02.032.
13. Ahmed, A. Imaging of the Paediatric Paranasal Sinuses. *South African Journal of Radiology* **2013**, *17*, 91–97, doi:10.4102/sajr.v17i3.273.
14. Lee, S.; Fernandez, J.; Mirjalili, S.A.; Kirkpatrick, J. Pediatric Paranasal Sinuses—Development, Growth, Pathology, & Functional Endoscopic Sinus Surgery. *Clinical Anatomy* 2022, *35*, 745–761.
15. Stenner, M.; Rudack, C. Diseases of the Nose and Paranasal Sinuses in Child. *GMS Curr. Top. Otorhinolaryngol. Head Neck Surg.* **2014**, *13*, Doc10, doi:10.3205/cto000113.
16. Badr, D.T.; Gaffin, J.M.; Phipatanakul, W. Pediatric Rhinosinusitis. *Curr. Treat. Options Allergy* 2016, *3*, 268–281.
17. Quintanilla-Dieck, L.; Lam, D.J. Chronic Rhinosinusitis in Children. *Curr. Treat. Options Pediatr.* **2018**, *4*, 413–424, doi:10.1007/s40746-018-0142-z.
18. Fokkens, W.J.; Lund, V.J.; Hopkins, C.; Hellings, P.W.; Kern, R.; Reitsma, S.; Toppila-Salmi, S.; Bernal-Sprekelsen, M.; Mullol, J.; Alobid, I.; et al. European Position Paper on Rhinosinusitis and Nasal Polyps 2020. *Rhinology* **2020**, *58*, 1–464, doi:10.4193/Rhin20.600.
19. Fagundes, N.C.F.; Gianoni-Capenakas, S.; Heo, G.; Flores-Mir, C. Craniofacial Features in Children with Obstructive Sleep Apnea: A Systematic Review and Meta-Analysis. *Journal of Clinical Sleep Medicine* 2022, *18*, 1865–1875.
20. Bulut, A.; Aşkın, M.B.; Bulut, Ö.E. Global Trends in Pediatric Craniofacial Growth and Airway Physiology Research: Insights from a Five-Year Bibliometric Analysis. *Sleep and Breathing* **2026**, *30*, 155, doi:10.1007/s11325-026-03702-2.
21. Hill, D.B.; Button, B.; Rubinstein, M.; Boucher, R.C. PHYSIOLOGY AND PATHOPHYSIOLOGY OF HUMAN AIRWAYMUCUS. *Physiol. Rev.* 2022, *102*, 1757–1836.
22. Knowles, M.R.; Boucher, R.C. Mucus Clearance as a Primary Innate Defense Mechanism for Mammalian Airways. *Journal of Clinical Investigation* **2002**, *109*, 571–577, doi:10.1172/jci15217.
23. Chatterjee, M.; van Putten, J.P.M.; Strijbis, K. Defensive Properties of Mucin Glycoproteins during Respiratory Infections—Relevance for Sars-Cov-2. *mBio* **2020**, *11*, 1–12, doi:10.1128/mBio.02374-20.
24. Wood, P.B.; Nagy, E.; Pearson, F.G.; Rae, S. MEASUREMENT OF MUCOCILIARY CLEARANCE FROM THE LOWER RESPIRATORY TRACT OF NORMAL DOGS. *Can Anaesth Soc J* **1973**, 192–206, doi:doi:10.1007/BF03027208.

 doi:10.20944/preprints202605.1331.v1

25. Button, B.; Cai, L.H.; Ehre, C.; Kesimer, M.; Hill, D.B.; Sheehan, J.K.; Boucher, R.C.; Rubinstein, M. A Periciliary Brush Promotes the Lung Health by Separating the Mucus Layer from Airway Epithelia. *Science (1979).* **2012**, *337*, 937–941, doi:10.1126/science.1223012.
26. Weibel, E.R. Morphometry of the Human Lung: The State of the Art after Two Decades. *Clinical Respiratory Physiology* 1979, *15*, 999–1013.
27. McShane, A.; Bath, J.; Jaramillo, A.M.; Ridley, C.; Walsh, A.A.; Evans, C.M.; Thornton, D.J.; Ribbeck, K. Mucus. *Current Biology* **2021**, *31*, R938–R945, doi:10.1016/j.cub.2021.06.093.
28. Hill, D.B.; Vasquez, P.A.; Mellnik, J.; McKinley, S.A.; Vose, A.; Mu, F.; Henderson, A.G.; Donaldson, S.H.; Alexis, N.E.; Boucher, R.C.; et al. A Biophysical Basis for Mucus Solids Concentration as a Candidate Biomarker for Airways Disease. *PLoS One* **2014**, *9*, doi:10.1371/journal.pone.0087681.
29. Thornton, D.J.; Rousseau, K.; McGuckin, M.A. Structure and Function of the Polymeric Mucins in Airways Mucus. *Annu. Rev. Physiol.* 2008, *70*, 459–486.
30. Bonser, L.R.; Erle, D.J. Airway Mucus and Asthma: The Role of MUC5AC and MUC5B. *J. Clin. Med.* 2017, *6*.
31. Aksamit, T.R.; O'Donnell, A.E.; Barker, A.; Olivier, K.N.; Winthrop, K.L.; Daniels, M.L.A.; Johnson, M.; Eden, E.; Griffith, D.; Knowles, M.; et al. Adult Patients With Bronchiectasis: A First Look at the US Bronchiectasis Research Registry. *Chest* **2017**, *151*, 982–992, doi:10.1016/j.chest.2016.10.055.
32. Rose, M.C.; Voynow, J.A. Respiratory Tract Mucin Genes and Mucin Glycoproteins in Health and Disease. *Physiol. Rev.* 2006, *86*, 245–278.
33. Nevitt, S.J.; Thornton, J.; Murray, C.S.; Dwyer, T. Inhaled Mannitol for Cystic Fibrosis. *Cochrane Database of Systematic Reviews* 2018, *2018*.
34. Zhou, X.; Kinlough, C.L.; Hughey, R.P.; Jin, M.; Inoue, H.; Etling, E.; Modena, B.D.; Kaminski, N.; Bleecker, E.R.; Meyers, D.A.; et al. Sialylation of MUC4β N-Glycans by ST6GAL1 Orchestrates Human Airway Epithelial Cell Differentiation Associated with Type-2 Inflammation. *JCI Insight* **2019**, *4*, doi:10.1172/jci.insight.122475.
35. Widdicombe, J.H.; Wine, J.J. Airway Gland Structure and Function. *Physiol. Rev.* **2015**, *95*, 1241–1319, doi:10.1152/physrev.00039.2014.
36. Sturgess, J.; Reid, L. Secretory Activity of the Human Bronchial Mucous Glands in Vitro. *Exp. Mol. Pathol.* **1972**, *16*, 362–381, doi:10.1016/0014-4800(72)90011-1.
37. Okuda, K.; Chen, G.; Subramani, D.B.; Wolf, M.; Gilmore, R.C.; Kato, T.; Radicioni, G.; Kesimer, M.; Chua, M.; Dang, H.; et al. Localization of Secretory Mucins MUC5AC and MUC5B in Normal/Healthy Human Airways. *Am. J. Respir. Crit. Care Med.* **2019**, *199*, 715–727, doi:10.1164/rccm.201804-0734OC.
38. Davis, C.W.; Dickey, B.F. Regulated Airway Goblet Cell Mucin Secretion. *Annu. Rev. Physiol.* 2008, *70*, 487–512.
39. Kanoh, S.; Tanabe, T.; Rubin, B.K. IL-13-Induced MUC5AC Production and Goblet Cell Differentiation Is Steroid Resistant in Human Airway Cells. *Clinical and Experimental Allergy* **2011**, *41*, 1747–1756, doi:10.1111/j.1365-2222.2011.03852.x.
40. Radicioni, G.; Ceppe, A.; Ford, A.A.; Alexis, N.E.; Barr, R.G.; Bleecker, E.R.; Christenson, S.A.; Cooper, C.B.; Han, M.L.K.; Hansel, N.N.; et al. Airway Mucin MUC5AC and MUC5B Concentrations and the Initiation and Progression of Chronic Obstructive Pulmonary Disease: An Analysis of the SPIROMICS Cohort. *Lancet Respir. Med.* **2021**, *9*, 1241–1254, doi:10.1016/S2213-2600(21)00079-5.
41. Chen, Y.; Garvin, L.M.; Nickola, T.J.; Watson, A.M.; Colberg-Poley, A.M.; Rose, M.C. IL-1β Induction of MUC5AC Gene Expression Is Mediated by CREB and NF-KB and Repressed by Dexamethasone. *Am. J. Physiol. Lung Cell. Mol. Physiol.* **2014**, *306*, doi:10.1152/ajplung.00347.2013.
42. Henderson, A.G.; Ehre, C.; Button, B.; Abdullah, L.H.; Cai, L.H.; Leigh, M.W.; DeMaria, G.C.; Matsui, H.; Donaldson, S.H.; Davis, C.W.; et al. Cystic Fibrosis Airway Secretions Exhibit Mucin Hyperconcentration and Increased Osmotic Pressure. *Journal of Clinical Investigation* **2014**, *124*, 3047–3060, doi:10.1172/JCI73469.
43. Anderson, W.H.; Coakley, R.D.; Button, B.; Henderson, A.G.; Zeman, K.L.; Alexis, N.E.; Peden, D.B.; Lazarowski, E.R.; Davis, C.W.; Bailey, S.; et al. The Relationship of Mucus Concentration (Hydration) to Mucus Osmotic Pressure and Transport in Chronic Bronchitis. *Am. J. Respir. Crit. Care Med.* **2015**, *192*, 182–190, doi:10.1164/rccm.201412-2230OC.

 doi:10.20944/preprints202605.1331.v1

44. Kesimer, M.; Ford, A.A.; Ceppe, A.; Radicioni, G.; Cao, R.; Davis, C.W.; Doerschuk, C.M.; Alexis, N.E.; Anderson, W.H.; Henderson, A.G.; et al. Airway Mucin Concentration as a Marker of Chronic Bronchitis. *New England Journal of Medicine* **2017**, *377*, 911–922, doi:10.1056/nejmoa1701632.
45. Wagner, C.E.; Wheeler, K.M.; Ribbeck, K. Mucins and Their Role in Shaping the Functions of Mucus Barriers. *Annu. Rev. Cell Dev. Biol.* **2018**, *34*, 189–215, doi:10.1146/annurev-cellbio-100617-062818.
46. Bakshani, C.R.; Morales-Garcia, A.L.; Althaus, M.; Wilcox, M.D.; Pearson, J.P.; Bythell, J.C.; Burgess, J.G. Evolutionary Conservation of the Antimicrobial Function of Mucus: A First Defence against Infection. *NPJ Biofilms Microbiomes* 2018, *4*.
47. Markovetz, M.R.; Subramani, D.B.; Kissner, W.J.; Morrison, C.B.; Garbarine, I.C.; Ghio, A.; Ramsey, K.A.; Arora, H.; Kumar, P.; Nix, D.B.; et al. Endotracheal Tube Mucus as a Source of Airway Mucus for Rheological Study. *Am. J. Physiol. Lung Cell. Mol. Physiol.* **2019**, *317*, L498–L509, doi:10.1152/AJPLUNG.00238.2019.
48. Button, B.; Goodell, H.P.; Atieh, E.; Chen, Y.C.; Williams, R.; Shenoy, S.; Lackey, E.; Shenkute, N.T.; Cai, L.H.; Dennis, R.G.; et al. Roles of Mucus Adhesion and Cohesion in Cough Clearance. *Proc. Natl. Acad. Sci. U. S. A.* **2018**, *115*, 12501–12506, doi:10.1073/pnas.1811787115.
49. Haas, A. Rapid Expansion Of The Maxillary Dental Arch And Nasal Cavity By Opening The Midpalatal Suture. *Angle Orthod.* 1961, *31*, 73–90.
50. Hicks, E.P. Slow Maxillary Expansion. A Clinical Study of the Skeletal versus Dental Response to Low-Magnitude Force. *Am. J. Orthod.* **1978**, *73*, 121–141, doi:10.1016/0002-9416(78)90183-5.
51. Jafari, A.; Shetty, K.S.; Kumar, M. Study of Stress Distribution and Displacement of Various Craniofacial Structures Following Application of Transverse Orthopedic Forces - A Three-Dimensional FEM Study. *Angle Orthodontist* **2003**, *73*, 12–20, doi:10.1043/0003-3219(2003)073<0012:SOSDAD>2.0.CO;2.
52. Gautam, P.; Valiathan, A.; Adhikari, R. Stress and Displacement Patterns in the Craniofacial Skeleton with Rapid Maxillary Expansion: A Finite Element Method Study. *American Journal of Orthodontics and Dentofacial Orthopedics* **2007**, *132*, 5.e1-5.e11, doi:10.1016/j.ajodo.2006.09.044.
53. Priyadarshini, J.; Mahesh, C.M.; Chandrashekar, B.S.; Sundara, A.; Arun, A. V.; Reddy, V.P. Stress and Displacement Patterns in the Craniofacial Skeleton with Rapid Maxillary Expansion—a Finite Element Method Study. *Prog. Orthod.* **2017**, *18*, doi:10.1186/s40510-017-0172-2.
54. Lo Giudice, A.; Polizzi, A.; Lagravere, M.; Flores-Mir, C.; Isola, G.; Ronsivalle, V.; Leonardi, R. Changes in Upper Airway Airflow after Rapid Maxillary Expansion Considering Normal Craniofacial Development as a Factor: A Retrospective Study Using Computer Fluid Dynamics. *Eur. J. Orthod.* **2025**, *47*, doi:10.1093/ejo/cjae077.
55. MacGinnis, M.; Chu, H.; Youssef, G.; Wu, K.W.; Machado, A.W. ilson; Moon, W. The Effects of Micro-Implant Assisted Rapid Palatal Expansion (MARPE) on the Nasomaxillary Complex--a Finite Element Method (FEM) Analysis. *Prog. Orthod.* **2014**, *15*, 52, doi:10.1186/s40510-014-0052-y.
56. Lee, S.C.; Park, J.H.; Bayome, M.; Kim, K.B.; Araujo, E.A.; Kook, Y.A. Effect of Bone-Borne Rapid Maxillary Expanders with and without Surgical Assistance on the Craniofacial Structures Using Finite Element Analysis. *American Journal of Orthodontics and Dentofacial Orthopedics* **2014**, *145*, 638–648, doi:10.1016/j.ajodo.2013.12.029.
57. Rees, J.S.; Jacobsen, P.H. Elastic Modulus of the Periodontal Ligament. *Biomaterials* **1997**, *18*, 995–999, doi:10.1016/S0142-9612(97)00021-5.
58. Ruse, N.D. Propagation of Erroneous Data for the Modulus of Elasticity of Periodontal Ligament and Gutta Percha in FEM/FEA Papers: A Story of Broken Links. *Dental Materials* **2008**, *24*, 1717–1719, doi:10.1016/j.dental.2008.04.006.
59. Vaida, L.; Moldovan, L.; Lile, I.E.; Todor, B.I.; Porumb, A.; Tig, I.; Bratu, D.C. A Comparative Study on Mechanical Properties of Some Thermoplastic and Thermo Set Resins Used for Orthodontic Appliances. *Materiale Plastice* **2015**, *52*, 364–367.
60. Attinger, D.; Moore, C.; Donaldson, A.; Jafari, A.; Stone, H.A. Fluid Dynamics Topics in Bloodstain Pattern Analysis: Comparative Review and Research Opportunities. *Forensic Sci. Int.* **2013**, *231*, 375–396, doi:10.1016/j.forsciint.2013.04.018.

 doi:10.20944/preprints202605.1331.v1

61. Boryor, A.; Hohmann, A.; Wunderlich, A.; Geiger, M.; Kilic, F.; Sander, M.; Sander, C.; Böckers, T.; Günter Sander, F. In-Vitro Results of Rapid Maxillary Expansion on Adults Compared with Finite Element Simulations. *J. Biomech.* **2010**, *43*, 1237–1242, doi:10.1016/j.jbiomech.2010.02.002.
62. Angelieri, F.; Cevidanes, L.H.S.; Franchi, L.; Gonçalves, J.R.; Benavides, E.; McNamara, J.A. Midpalatal Suture Maturation: Classification Method for Individual Assessment before Rapid Maxillary Expansion. *American Journal of Orthodontics and Dentofacial Orthopedics* **2013**, *144*, 759–769, doi:10.1016/j.ajodo.2013.04.022.
63. Tanaka, O.M.; Araújo, E.A.; Oliver, D.R.; Behrents, R.G. A Finite Element Analysis of the Maxillary First Molar PDL with Maxillary Protraction in a Mixed Dentition Class III Malocclusion. *Orthod. Craniofac. Res.* **2015**, *18*, 242–250, doi:10.1111/ocr.12102.
64. Tanaka, O.M.; Saga, A.Y.; Pithon, M.M.; Argenta, M.A. Stresses in the Midpalatal Suture in the Maxillary Protraction Therapy: A 3D Finite Element Analysis. *Prog. Orthod.* **2016**, *17*, doi:10.1186/s40510-016-0121-5.
65. Mitani, Y.; Banabilh, S.M.; Singh, G.D. Craniofacial Changes in Patients with Class III Malocclusion Treated with the RAMPA System. *Int. J. Orthod. Milwaukee* **2010**, *21*, 19–25.
66. Mitani, Y.; Choi, B.; Choi, J. Anterosuperior Protraction of Maxillae Using the Extraoral Device, RAMPA; Finite Element Method. *Comput. Methods Biomech. Biomed. Engin.* **2018**, *21*, 722–729, doi:10.1080/10255842.2018.1514498.
67. Moshfeghi, M.; Mitani, Y.; Choi, B.; Emamy, P. Finite Element Simulations of the Effects of an Extraoral Device, RAMPA, on Anterosuperior Protraction of the Maxilla and Comparison with GHu-1 Intraoral Device. *Angle Orthod.* **2021**, *91*, 804–814, doi:10.2319/020521-106.1.
68. Moshfeghi, M.; Mitani, Y.; Okai-Kojima, Y.; Choi, B.; Emamy, P. RAMPA Therapy: Impact of Suture Stiffness on the Anterosuperior Protraction of Maxillae; Finite Element Analysis. *Oral — Health, Diseases, Therapies, and Technologies* **2025**, *5*, doi:10.3390/oral5040074.
69. Mitani, Y.; Okai-Kojima, Y.; Moshfeghi, M.; Morio, T.; Ogisawa, S.; Choi, B. CBCT Volumetric Changes in Combined Nasal Cavity and Paranasal Sinuses Following RAMPA-ROA Therapy: A Retrospective Cohort Study with Reference to Longitudinal Growth Data. *J. Clin. Med.* **2026**, *15*, doi:10.3390/jcm15072605.
70. Mitani, Y.; Okai-Kojima, Y.; Moshfeghi, M.; Tonogi, M.; Ogisawa, S.; Choi, B. The Effect of RAMPA Therapy on the Volumetric Evaluation of the Nasal Cavity and Sinus: A Comparative Statistical Analysis in Patients with Clear Versus Opacified Paranasal Sinuses. *Oral* **2026**, *6*, 8, doi:10.3390/oral6010008.
71. Moshfeghi, M.; Mitani, Y.; Okai-Kojima, Y.; Choi, B. Impact of RAMPA Therapy on Nasal Cavity Expansion and Paranasal Drainage: Fluid Mechanics Analysis, CAE Simulation, and a Case Study. *Biomimetics* **2025**, *11*, 5, doi:10.3390/biomimetics11010005.
72. Mitani, Y.; Moshfeghi, M.; Kumamoto, N.; Choi, B. Finite Element and Clinical Analyses of Effects of a New Intraoral Device (VomPress) Combined with Extraoral RAMPA on Improving the Overjet of Craniofacial Complex. *Comput. Methods Biomech. Biomed. Engin.* **2022**, *25*, 1099–1110, doi:10.1080/10255842.2021.2001803.